J Biol Inorg Chem (2006) 11: 307–315
DOI 10.1007/s00775-005-0077-2

ORIGINAL PAPER

Pedro M. Rodrigues · Anjos L. Macedo
Brian J. Goodfellow · Isabel Moura · José J. G. Moura

Desulfovibrio gigas ferredoxin II: redox structural modulation of the [3Fe–4S] cluster

Received: 22 July 2005 / Accepted: 22 December 2005 / Published online: 2 February 2006

Abstract *Desulfovibrio gigas* ferredoxin II (*Dg*FdII) is a small protein with a polypeptide chain composed of 58 amino acids, containing one Fe_3S_4 cluster per monomer. Upon studying the redox cycle of this protein, we detected a stable intermediate ($FdII_{int}$) with four ^1H resonances at 24.1, 20.5, 20.8 and 13.7 ppm. The differences between $FdII_{ox}$ and $FdII_{int}$ were attributed to conformational changes resulting from the breaking/formation of an internal disulfide bridge. The same ^1H NMR methodology used to fully assign the three cysteinyl ligands of the [3Fe–4S] core in the oxidized state ($DgFdII_{ox}$) was used here for the assignment of the same three ligands in the intermediate state ($DgFdII_{int}$). The spin-coupling model used for the oxidized form of *Dg*FdII where magnetic exchange coupling constants of around 300 cm^{-1} and hyperfine coupling constants equal to 1 MHz for all the three iron centres were found, does not explain the isotropic shift temperature dependence for the three cysteinyl cluster ligands in $DgFdII_{int}$. This study, together with the spin delocalization mechanism proposed here for $DgFdII_{int}$, allows the detection of structural modifications at the [3Fe-4S] cluster in $DgFdII_{ox}$ and $DgFdII_{int}$.

Keywords Fe_3S_4 cluster · Ferredoxin · Disulfide bridge · Paramagnetic protein · *Desulfovibrio gigas*

P. M. Rodrigues
FCMA, CCMAR, Universidade do Algarve,
Campus de Gambelas, 8005-139 Faro, Portugal

A. L. Macedo · I. Moura · J. J. G. Moura (✉)
REQUIMTE, Departamento de Química,
Centro de Química Fina e Biotecnologia,
Faculdade de Ciências e Tecnologia,
Universidade Nova de Lisboa, 2829-516 Caparica,
Portugal
E-mail: jose.moura@dq.fct.unl.pt
Tel.: +351-21-2954464
Fax: +351-21-2948550

B. J. Goodfellow
Departamento de Química, Universidade de Aveiro,
3810 Aveiro, Portugal

Abbreviations *Dg*: *Desulfovibrio gigas* · Fd: Ferredoxin · NOE: Nuclear Overhauser effect · NOESY: Nuclear Overhauser enhancement spectroscopy · SRB: Sulfate-reducing bacteria

Introduction

Ferredoxins (Fds) are simple electron transfer proteins with iron and sulfide at the active site, with cysteinyl sulfur atoms as cluster terminal ligands (other atoms, such as O or N, may be involved) [1]. Since the discovery of these proteins 40 years ago, many other proteins containing [Fe–S] clusters of distinct types have been discovered [2–4]. The existence of different types of [Fe–S] proteins and clusters points to a remarkable functional and structural diversity, reflecting the chemical versatility of both iron and sulfur [3, 4]. The known functions of biological [Fe–S] clusters include electron transfer in Fds and redox enzymes [1, 5–7], coupled electron/proton transfer [8], substrate binding and activation [9–19], Fe or cluster storage [20], structural control [21–23], regulation of gene expression [24–31] and enzyme activity [32–34], disulfide reduction [35–37] and sulfur donation [38–40].

Four distinct types of Fds are found in sulfate-reducing bacteria (SRB), where they play a relevant metabolic role: 3Fe Fd containing one [3Fe–4S], 4Fe Fd containing one [4Fe–4S], 7Fe Fd containing a [3Fe–4S] and a [4Fe–4S] cluster, and 8Fe Fd containing two [4Fe–4S] clusters [41].

Desulfovibrio gigas (*Dg*) FdII is a small protein, of 58 amino acids with 1 [3Fe–4S] cluster per monomer [42, 43] investigations. In the native state the protein is a tetramer. The three-dimensional structure has already been established by X-ray [44] and also by NMR [45]. Cys8, Cys14 and Cys50 bind the cluster; Cys11 is available to bind the fourth ligand in FdI that contains a [4Fe–4S] cluster. The two remaining cysteines, Cys18 and Cys42, form a disulfide bridge in the native state [44, 46]. *Dg*FdII can be converted to FdI following incubation with excess

Fe^{2+} in the presence of dithiothreitol [47], showing that the polypeptide chain of *Dg*Fd can accommodate both [3Fe–4S] and [4Fe–4S] clusters. This cluster interconversion leads to the incorporation of other transition metals into the [3Fe–4S] cluster, with the [Co, 3Fe–4S] heterometal centre in *Dg*FdII being the first reported [48], and similar results were subsequently found for *D. africanus* FdIII [49] and *Pyrococcus furiosus* Fd [50]. Other [Zn, 3Fe–4S] and [Ni, 3Fe–4S] centres were also produced from this protein [51, 52]. This interconversion mechanism and the cluster geometries appear to have physiological significance between the oxidized and reduced states. Recently, the crystallization of *Dg*FdII under an anaerobic environment gave crystals which diffracted at a resolution of 1.37 Å [53].

The [3Fe–4S] cluster can be stabilized in two oxidation states: $[3Fe–4S]^{+}$ and $[3Fe–4S]^{0}$. In the oxidized state, the three high-spin ferric atoms ($S=5/2$) are antiferromagnetically coupled, forming a ground electronic state with a global spin of 1/2 [54]. One-electron reduction gives an $S=2$ state, resulting from the antiferromagnetic coupling between a delocalized iron pair ($S=9/2$), that share the incoming electron, and a high-spin iron(III) site ($S=5/2$), as indicated by Mössbauer investigations [47, 55, 56]. Electrochemical studies of the 7Fe Fds from *D. africanus* FdIII [49, 57], *Azotobacter vinelandii* FdI [58] and *Sulfolobulus acidocaldarius* [59] suggest that further reduction of the cluster leads to a formal $[3Fe–4S]^{2-}$ oxidation state. Similar observations of the detection of an all-ferrous state were also reported for *Dg*FdII [52] and the 3Fe interconverted form of *P. furiosus* Fd [60].

The specific assignment of the β-CH_2 protons of the cysteinyl cluster ligands was made, for $FdII_{ox}$, by ^1H NMR [61, 62]. These protons are affected by the cluster paramagnetism and their chemical shift temperature dependence was used to study the electronic properties of the cluster. On the basis of the coupling model for the cluster iron atoms [63, 64], the NMR data allowed the determination of the iron coupling constants [62]. The temperature dependence of these β-CH_2 protons showed one pair could be assigned to Cys50 with Curie dependence and the other two pairs belonged to Cys8 and Cys14 with anti-Curie behaviour [61, 62]. This can be explained assuming different exchange coupling interactions between the three iron atoms that coordinate the cysteines, with $J_{13}=J_{23}=J$ and $J_{12}=J+\Delta J$ ($\Delta J>0$). Values of $J\approx300$ cm^{-1} and $\Delta J/J\approx0.02$ were found to fit the experimental data [62]. The reported J values that better reproduce the experimental NMR data for both the [3Fe–4S] clusters of the Fe_7S_8 Fds from *Bacillus schlegelii* [65] and *Rhodopseudomonas palustris* [66] were also determined and were found to be around 300 cm^{-1}. The J values determined were, respectively, $J_{12}=320$, $J_{23}=280$ and $J_{13}=290$ cm^{-1} for *B. schlegelii* and $J_{12}=285$, $J_{13}=300$ and $J_{23}=320$ cm^{-1} for *R. palustris*. Comparing these values with those for *Dg*FdII we can observe that the magnetic interaction within the [3Fe–4S] cluster is less symmetric in Fe_7S_8 Fds, agreeing with the fact that in those last two cases, one cysteinyl β-CH_2 proton displays an upfield-shifted signal that is not present in the single-cluster FdII protein from *Dg* [62].

NMR also proved to be a very sensitive tool to detect structural alterations, allowing the detection of a stable intermediate state ($FdII_{int}$) in the potential range around −130 mV, where the cluster is reduced from the +1 to the 0 state [46]. $FdII_{int}$ was characterized by Mössbauer and electron paramagnetic resonance techniques, showing that the [3Fe–4S] cluster remains in the oxidized state [47]. The differences in the NMR and Mössbauer spectra between $FdII_{ox}$ and $FdII_{int}$ were due to conformational changes resulting from the breaking/formation of the disulfide bridge. The same intermediate state was found later in the *P. furiosus* 4Fe Fd [67]. This may turn out to be a key observation for the mechanism of complex proteins containing iron–sulfur clusters.

We will present a characterization of that intermediate state ($FdII_{int}$) in terms of the electronic properties of the cluster and structural rearrangements of the cluster vicinity, using NMR spectroscopy.

Materials and methods

Protein purification

*Dg*FdII was purified as previously described [42] with a slight modification: the last purification step was performed in a gel filtration prepacked Pharmacia column (Superdex 75 HR 10/30) by high-performance liquid chromatography, and elution was made with 50 mM phosphate buffer at pH 7.6 with NaCl 150 mM. The purified protein solutions were simultaneously concentrated, equilibrated with 100 mM phosphate buffer at pH 8.0 and exchanged with 99.9% D_2O using AMICON centricons with a 5-kDa cutoff.

Sample preparation

The intermediate state, $FdII_{int}$, was generated by adding proper amounts of sodium dithionite to the native protein under anaerobic conditions. EDTA was present to prevent [4Fe–4S] cluster formation.

NMR experiments

High-resolution NMR spectra were recorded either with 400-MHz ARX or 600-MHz AMX Fourier transform Bruker spectrometers equipped with a temperature-control unit. Chemical shift values are quoted in parts per million relative to 3-trimethylsilyl-(2,2,3,3-$^2H_4$) propionate. Positive values refer to low-field shifts. T_1 measurements were made using the inversion-recovery method [68]. The proton nuclear Overhauser effect (NOE) experiments were performed either at 400 MHz or at 600 MHz using the super-WEFT pulse sequence

(180-τ-90-AQ) [69] with τ values and recycle times, 100–200 ms, providing water suppression. Selective saturation of the resonances was made during the delay time τ. Difference spectra were obtained by subtracting the off-resonance spectra from the on-resonance spectra, as described in Ref. [70]. Two-dimensional experiments were carried out at 400 MHz. Phase-sensitive nuclear Overhauser enhancement spectroscopy (NOESY) [71, 72] spectra were recorded with mixing times around 5 ms, with 1,024 t_2 points and 256 t_1 increments and 3,000–4,000 scans per increment. Repetition times were 75–100 ms. In the processing, before Fourier transformation the data were multiplied by an unshifted sine-bell window function in the f_2 dimension and an unshifted sine-bell window function in the f_1 dimension.

Results

The intermediate state obtained by dithionite reduction of the native *Dg*FdII is stable for several days, allowing NMR techniques to be easily applied. This state is characterized by a $[3Fe–4S]^+$ centre and a broken S–S bridge between Cys18 and Cys42. Both $FdII_{ox}$ and $FdII_{int}$ states have a paramagnetic cluster with $S=1/2$, affecting the properties of the resonances for the protons of the ligands bound to the iron atom and those protons within about 8 Å of the cluster [46].

Figure 1 presents the ^{1}H NMR spectrum of a *Dg*FdII sample where the protein is in equilibrium between the oxidized and intermediate states. As previously reported [61], $FdII_{ox}$ displays four broad resonances at 29.3, 24.4, 16.8 and 15.3 ppm, in the low-field region of the spectrum. These resonances (labelled a–d in Fig. 1) were assigned to the β-CH_2 protons of the three cysteinyl cluster ligands. The sequence-specific assignments are presented in Table 1. Resonance a shows a correlation

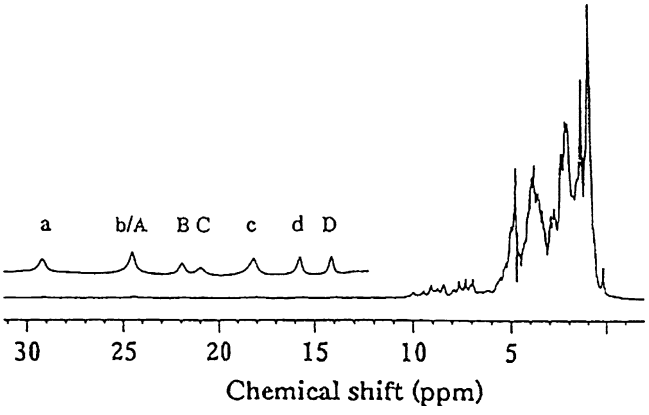

Fig. 1 Complete 400-MHz ^{1}H NMR spectrum (with water suppression) of a mixture of *Desulfovibrio gigas* (*Dg*) ferredoxin (*Fd*) II_{ox}/*Dg*$FdII_{int}$ in ^2H_2O (pH 8.0) at 310 K. The upper expanded low-field region has resonances labelled *a–d* and *A–D*, belonging to the oxidized and intermediate states of *Dg*FdII, respectively. There is 54% of the mixture in the oxidized state and 46% in the intermediate state. No reduced state was detected

with a resonance at 4.1 ppm in the ^{1}H NOESY spectrum, with a 10 ms mixing time at 303 K (not shown), that can be assigned to the α-CH proton of Cys50, based on the cross-peak intensity. All the protons of the cysteinyl cluster ligands for $FdII_{ox}$ have therefore now been sequence-specifically assigned.

The resonances in the low-field region, between 25 and 12 ppm labelled A–D, belong to the protons of the cysteinyl cluster ligands of the intermediate state. The temperature behaviour and assignment of these resonances was carried out using ^{1}H NOESY experiments, performed with different mixing times (2–10 ms) and at different temperatures (290–310 K).

The connectivities detected in the 8-ms NOESY spectrum of a mixture of $FdII_{ox}$ (40%)/$FdII_{int}$ (60%) are shown in Fig. 2. The percentage of each species was estimated by integrating peaks d and D from the oxidized and intermediate states, respectively. The connectivities detected between resonances A and C, B and a resonance at 8.7 ppm, and D and a resonance at 7.8 ppm allow these resonances to be assigned to the three β-CH_2 protons of the cysteinyl cluster ligands, in the intermediate state. Resonance B also shows a correlation with a resonance at 1.4 ppm, as does resonance D with a resonance at 9.8 ppm. On the basis of the intensity of the observed cross peaks and the T_1 value (T_1 values for resonances A–D and the resonance at 9.8 ppm are listed in Table 1) for the resonance at 9.8 ppm, we can assign both 1.4- and 9.8-ppm resonances to α-CH protons.

In order to attempt the sequence-specific assignment of the hyperfine shifted resonances, one-dimensional NOE difference experiments were carried out for $FdII_{int}$. The experiment (not shown) allowed the specific assignment of peak D and the peak at 7.8 ppm to the β-CH_2 protons of Cys14. Saturation of peak D showed a NOE effect with the proton resonances of the aromatic ring of Phe22, which have been previously assigned [61]. Using the X-ray coordinates [44], Phe22, the only aromatic residue present in the protein, is close enough (3–4.7 Å for one β-CH_2 and 5–5.5 Å for the other) to display a NOE effect with β-CH_2 protons of Cys14. The one-dimensional NOE experiments when the other hyperfine shifted peaks were irradiated did not show any extra NOEs apart from those for their β-CH_2 or α-CH partner.

The temperature dependencies of the chemical shifts of the three β-CH_2 pairs of cysteine protons for both the oxidized state (resonances a–d, 8.6 and 3.0 ppm) and the intermediate state (resonances A–D, 8.7 and 7.8 ppm) areplotted in Fig. 3. The resonances of the oxidized state attributed to the β-CH_2 protons of Cys50 have Curie dependence, while all the other β-CH_2 protons have anti-Curie dependence [61]. The intermediate state shows similar behaviour: resonance D and the resonance at 7.8 ppm (Cys14) have Curie temperature dependence, while resonances A–C and the resonance at 8.7 ppm have anti-Curie dependence. By comparing the chemical shifts and slopes of the temperature dependencies it was

Table 1 Summary of the NMR spectral parameters and assignment of the coordinated cysteinyl proton resonances, for both *Desulfovibrio gigas* (*Dg*) ferredoxin (*Fd*) II_{ox} and *Dg*$FdII_{int}$ at 300 K

Cys	Protons	*Dg*$FdII_{ox}$ [61]		*Dg*$FdII_{int}$	
		Signal (ppm)	T_1 (ms)	Signal (ppm)	T_1 (ms)
50	β-CH	a (29.3)	4.3	A (24.1)	3.6
	β-CH	b (24.4)	3.1	C (20.5)	3.0
	α-CH	(4.1)	ND	ND	ND
14	β-CH	d (15.3)	7.0	D (13.7)	5.8
	β-CH	(8.6)	ND	(7.8)	ND
	α-CH	(9.7)	ND	(9.8)	16.4
8	β-CH	c (16.8)	4.0	B (20.8)	3.2
	β-CH	(3.0)	ND	(8.7)	ND
	α-CH	(1.43)	ND	(1.4)	ND

ND not determined

possible to tentatively assign, for $FdII_{int}$, resonances A and C to the β-CH_2 protons of Cys50 and resonance B and the resonance at 8.7 ppm to Cys8. It is interesting to note that Cys14 now appears as the least shifted β-CH_2 proton resonance and displays Curie temperature behaviour.

In order to probe the structural changes at the cluster for $FdII_{int}$ a plot of the contact chemical shifts of the cysteinyl β-CH_2 protons versus the corresponding Fe–S–Cβ–Cα dihedral angles (θ) for 3Fe Fds was made (Fig. 4). The experimental chemical shifts available for the β-CH_2 protons of *Dg*FdII, *Thermococcus litoralis* 3Fe Fd [73, 74] and *A. vinelandii* 7Fe Fd [75] were used (after subtracting 2.8 ppm, the intrinsic diamagnetic chemical shift for a β-CH_2 proton, and assuming that the contact term is dominant) [76] together with the θ values from the X-ray crystal structures of *Dg* [44] and *A. vinelandii* [77, 78] Fds. *T. litoralis* 3Fe Fd was used in this fitting considering the similarity between the NMR data from this protein and those from *Dg*FdII. Owing to the absence of X-ray data for this protein, we used the θ values available

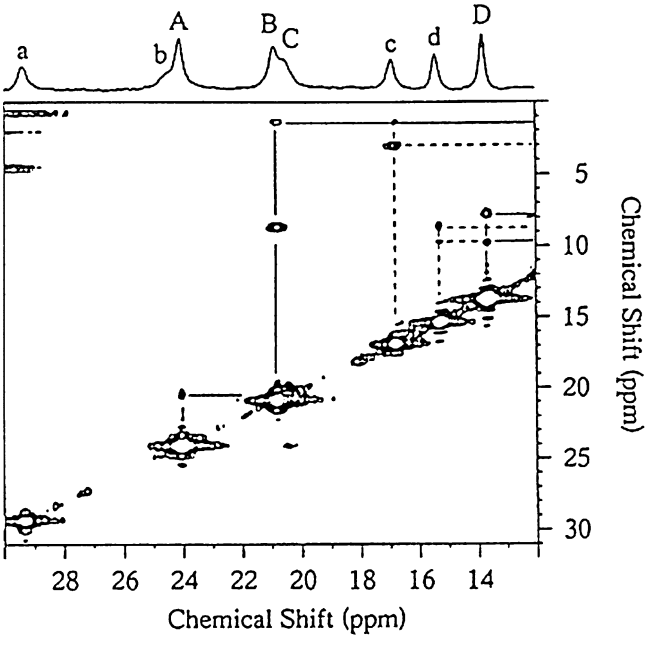

Fig. 2 The 400-MHz ^1H nuclear Overhauser enhancement spectroscopy (*NOESY*) (8-ms mixing time) NMR spectrum of a *Dg*$FdII_{ox}$/*Dg*$FdII_{int}$ mixture in ^2H_2O (pH 8.0) at 300 K. Connectivities for *Dg*$FdII_{ox}$ signals are indicated by *dashed lines*. Connectivities for *Dg*$FdII_{int}$ are represented by *solid lines*. Resonances in the one-dimensional ^1H NMR spectrum labelled *a–d* belong to the oxidized state and those labelled *A–D* to the intermediate state of the protein. The ratio of the oxidized state to the intermediate state was 40/60. No reduced state was detected

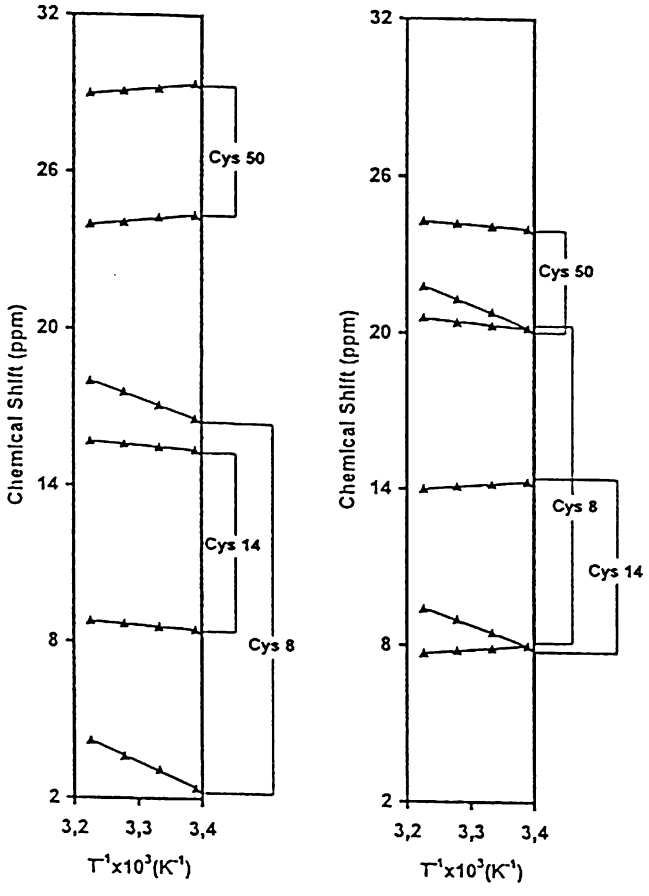

Fig. 3 Experimental temperature dependence of the isotropically shifted ^1H NMR signals of *Dg*$FdII_{ox}$ (*left*) and *Dg*$FdII_{int}$ (*right*) for the assigned cysteinyl residues Cys8, Cys14 and Cys50. The *solid lines* are not fits of the experimental data; they indicate the trends of the temperature dependencies only

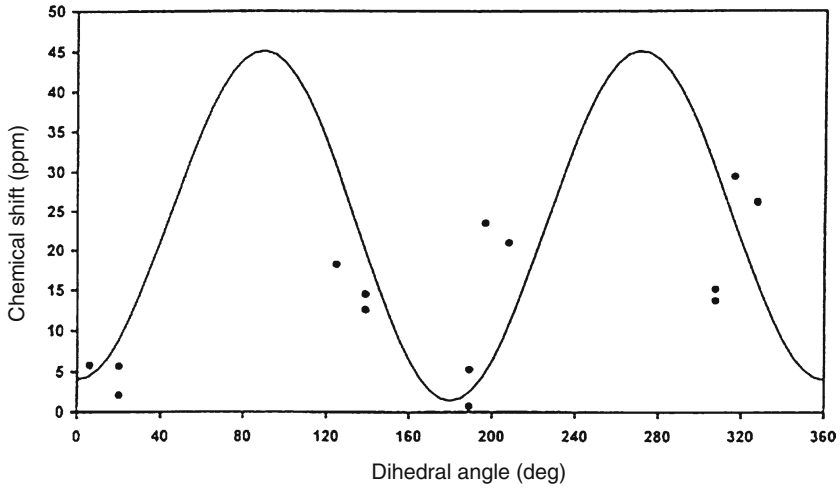

Fig. 4 Best fit for the modified version of the Karplus equation $\delta = a\sin^2\theta + b\cos\theta + c$ for the plot of the contact shifts of the cysteine β-CH_2 protons vs dihedral angles, θ, for [3Fe–4S] systems. The fitting values were $a = 41.87$, $b = -2.82$ and $c = 2.88$. A possible error was introduced in both chemical shift and dihedral angle variables. The values used for precision, chemical shift standard deviation and angle standard deviation were 0.01, 5.6 and 10, respectively. The experimental NMR chemical shifts used were those available for *Dg*FdII, *Thermococus litoralis* 3Fe Fd and *Azotobacter vinelandii* 7Fe Fd [54–56]. θ values were obtained from the X-ray structures of *Dg* and *A. vinelandii* Fds [31, 57, 58]

from the X-ray crystal structure of *Dg*FdII. The fitting was obtained using a modified version of Karplus equation $\delta = a\sin^2\theta + b\cos\theta + c$ [79], which accounts for both π and σ mechanisms of spin delocalization. A possible error in both chemical shift and dihedral angle variables was introduced, since the simulation program takes into account not only the angle error percentage arising from the X-ray structure, but also the error in the chemical shift for each proton of the three different cysteines. The best-fit values obtained for the three parameters gave values of 41.87, −2.82 and 2.88 for *a*, *b* and *c*, and 0.01, 5.6 and 10 for precision, chemical shift standard deviation and angle standard deviation, respectively.

We can obtain the dihedral angles for *Dg*$FdII_{int}$, by solving the Karplus equation with the values obtained for *a*, *b* and *c*, for each pair of protons of the three cysteines Cys8, Cys14 and Cys50, using the chemical shifts obtained experimentally for each of them. These values are presented in Table 2, and are compared with the θ values obtained from the *Dg*FdII crystal structure [44].

Table 2 Comparison of the dihedral angle (θ) Fe–S–Cα–Cβ values for *Dg*$FdII_{ox}$ and *Dg*$FdII_{int}$. The data were obtained from the X-ray structure for the oxidized state [31], and were extracted from the fitting presented in Fig. 4, for the intermediate state

Cys	Dihedral angle (degrees)	
	Dg$FdII_{ox}$	*Dg*$FdII_{int}$
8	68.3	261 ± 8
14	259.5	265 ± 20
50	87.7	268 ± 15

NOESY spectra, with 150-ms mixing times, were obtained for samples of $FdII_{ox}$, $FdII_{int}$ and fully reduced FdII, in order to study structural conformational changes in the protein, due to the opening of the disulfide bridge. Figure 5 shows the Hα/Hβ correlation region between Cys18 and Cys42 of the NOESY spectra obtained for the different redox states of the protein. It can be seen that the NOE found for the Hα Cys18/Hβ Cys42 cross peak in $FdII_{ox}$ (Fig. 5, panel a) is less intense in the intermediate state (where an equilibrium between oxidized and intermediate states is present; Fig. 5, panel b) and disappears in the fully reduced sample (where all the protein molecules have an open disulfide bridge; Fig. 5, panel c).

Discussion

In order to understand the alterations detected in the hyperfine shifted signals of the ^{1}H NMR spectrum of $FdII_{int}$ (Fig. 1), the sequence-specific assignments of the β-CH_2 protons of Cys8, Cys14 and Cys50 were first attempted. This was carried out using two-dimensional NOESY experiments with short mixing times (owing to the fast relaxation times of those protons affected by the cluster paramagnetism) and one-dimensional NOE experiments. The correlations obtained were described in the "Results" section, and are given in Table 1. It can be seen that the chemical shift of each β-CH_2 pair of protons does not change drastically when compared with the corresponding shifts for $FdII_{ox}$, and that the chemical shifts of the assigned α-CH protons (only detected for Cys8 and Cys14) are maintained. The sequence-specific assignment of Cys8 and Cys50 was carried out based on these observations. It is interesting

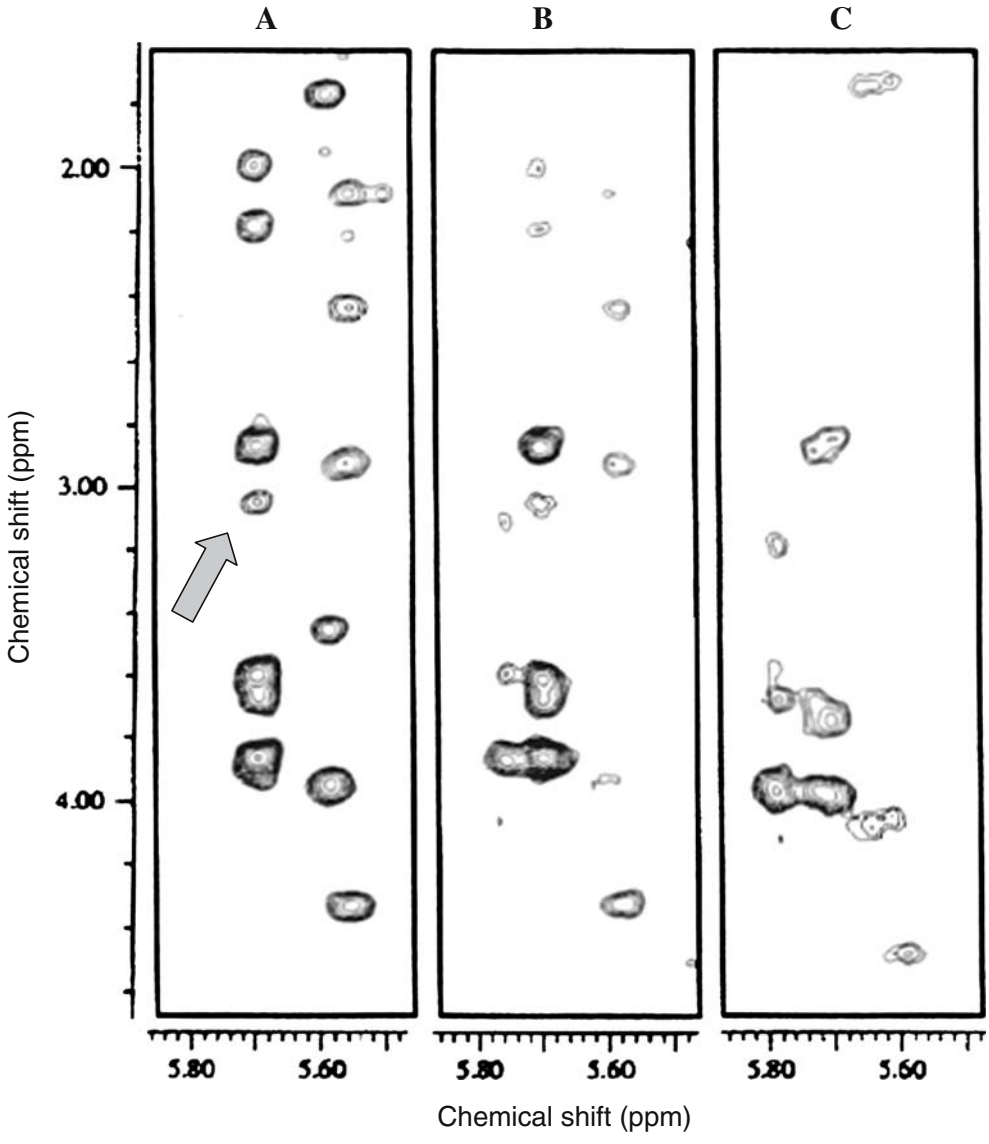

Fig. 5 A region of the 600-MHz ^{1}H NOESY (150-ms mixing time) NMR spectra of *Dg*FdII$_{ox}$ (*panel a*), *Dg*FdII$_{int}$ (*panel b*) and *Dg*FdII$_{red}$ (*panel c*), at 300 K. The *arrow* in (*panel a*) indicates the cross peak correlating the Hα proton of Cys18 with the Hβ proton of Cys42. In *panel b* this cross peak is less intense and disappears (*panel c*) when the protein is completely reduced

to note that the chemical shift spread of the β-CH$_2$ proton resonances is less for FdII$_{int}$ (they can be found between 8 and 24 ppm) compared with FdII$_{ox}$ (between 2 and 29 ppm). This suggests that rearrangements in the cluster environment, namely alterations in the dihedral angles Fe–S–Cβ–Cα or changes in the iron spin coupling in the cluster, due to the opening of the S–S bridge are taking place. It also suggests that the dihedral angles for the binding cysteines are becoming more equal on going from FdII$_{ox}$ to FdII$_{int}$ (if all the dihedral angles were the same all the β-CH$_2$ chemical shifts would be equal). The notion that the iron atoms are more equivalent in the intermediate state has already been discussed using results obtained from Mössbauer spectroscopy [46].

The temperature dependence of the three pairs of β-CH$_2$ resonances of the intermediate state (Fig. 3) displays typical behaviour that is found for all [3Fe–4S]$^+$ containing Fds, including *Dg*FdII$_{ox}$ [62]. The asymmetry found for the coupling between the three Fe^{3+} ($S=5/2$) atoms is reflected in the NMR spectrum by the presence of Curie temperature dependence for one of the bound cysteines and anti-Curie dependence for the remaining two. The difference found for FdII$_{int}$ is that it is no longer Cys50 that shows Curie behaviour [62]. Curie behaviour is now displayed by Cys14 and the parameters used in the spin-coupling model, already described for the oxidized form of *Dg*FdII [62], cannot explain the isotropic shift temperature dependencies of the three cysteinyl cluster ligands in FdII$_{int}$, as the 3Fe cluster is in the same oxidation state. A value of 300 cm^{-1} was estimated for the magnetic exchange coupling constants between the iron spins in FdII$_{ox}$ [42] with $J_{12}=J_{13}=J$, $J_{23}=J+\Delta J$ and $\Delta J/J=0.02$, using A values (coupling constant between the iron electronic spins and the β-CH$_2$ nuclear spins) of 1 MHz, for the three irons sites, as estimated for a [Fe–S] containing rubredoxin [80]. The set of J values found for the [3Fe–4S] cluster of the 7Fe *B. schlegelii* [45] and *R. palustris*

[66] Fds are also of the same order of magnitude as those found for *Dg*. Using *A* values of 1 MHz, Curie temperature dependence is always displayed (using different *J* and ΔJ values) by the cysteinyl β-CH_2 protons that have the larger chemical shifts. For $FdII_{int}$ the protons showing Curie dependence are those with the smaller chemical shifts (Cys14 using an average value for the β-CH_2 pair). This behaviour is only possible if different *A* values for each β-CH_2 chemical shift pair are introduced. This is supported by the fact that the slopes of the curves are maintained, and the curves are displaced by a factor that could result from a change in the *A* values. The Fe electron spin and ^1H nuclear spin coupling constant, *A*, is dependent on unpaired electron spin density at the ^1H nucleus and on the Fe–Sγ–Cβ–Cα dihedral angle. The observed change in temperature dependencies and chemical shifts could therefore result from either of these parameters. However, as the oxidation state of the [3Fe–4S] cluster is the same, +1, for $FdII_{ox}$ and $FdII_{int}$ no extra spin density appears to be present at the cluster. The change in temperature dependence and chemical shift, on going from $FdII_{ox}$ to $FdII_{int}$, must, then, result from a change in the dihedral angles at the cluster as a direct result of the loss of the S–S bridge between Cys18 and Cys42. The different distribution of spin density over the cluster caused/allowed by the change in dihedral angles is detected as changes in the chemical shift and temperature dependencies for the β-CH_2 protons (as the contact chemical shift is related to *A*).

With the data obtained when solving the Karplus equation, a positive value is found for parameter *a* (see "Materials and methods" section), indicating that the π mechanism of spin transfer is dominant, which is also the case for [4Fe–4S] systems. The curve in Fig. 4 was used to extract dihedral angle Fe–Sγ–Cα–Cβ information for $FdII_{int}$ as described in the "Results " section, and already applied to [4Fe–4S] containing Fds [76]. As can be seen in Table 2, the orientation of the β-CH_2 protons with respect to the cluster iron atoms is more or less maintained in $FdII_{int}$. However, as changes are seen in the chemical shifts, structural changes must be occurring at the cluster. It should be noted that small changes in the dihedral angles could cause large changes in the contact chemical shift. The actual difference seen for Cys14 is $5.5 \pm 20°$, while the differences for Cys8 and Cys50 are more significant, being $192.7 \pm 8°$ and $180.3 \pm 15°$, respectively. One possible explanation is that the Sγ atoms of Cys8 and Cys50 are both involved in NH–S H-bonds (NH–S: Ala10–Cys8, Ala31–Cys8, Ala52–Cys50 and Ala54–Cys50) in the X-ray structure. The NHs of both Cys8 and Cys50 are also involved in NH–O H-bonds, while the NH of Cys14 is not (it is 2.4 Å from a S atom).

Direct evidence for the loss of the S–S bridge between Cys18 and Cys42 on going from $FdII_{ox}$ to $FdII_{int}$ and finally to $FdII_{red}$, was obtained by the loss of intensity of the cross peak that correlates Hα Cys18/Hβ Cys42 found in a 150-ms NOESY spectrum (previously assigned in $FdII_{ox}$ [45]).

The cleavage of this S–S bridge is the catalyst that causes the structural changes that result in the modification of the cluster binding cysteine dihedral angles, which manifest themselves as changes in the chemical shifts and temperature dependencies of the β-CH_2 protons. It has recently been shown from the superimposition of the aerobic and anaerobic three-dimensional structures of *Dg*FdII [53] that the disulfide bond (Cys18–Cys42) in the aerobic structure has two conformations, which was also interpreted as an opening up of the covalent disulfide bond. Moreover, the Fe–S cluster geometry in the anaerobic structure is different from that in the aerobic structure, with a maximum increase and decrease of 0.15 and 0.14 Å for the Fe–S bond length ranges, respectively. A similar difference in the Fe–S cluster geometries was previously observed when recombinant *Dg*FdII was characterized spectroscopically [81]: differences in the paramagnetic envelope of the NMR spectra of both the recombinant and the native proteins already pointed to structural changes in the [3Fe–4S] cluster geometries.

Concluding remarks

NMR is a unique technique that can easily distinguish different redox states in Fe–S-containing proteins, giving information about the electronic structure of the cluster and detecting small alterations in the cluster environment as well as in the protein as a whole.

By using one-dimensional NOE experiments, two-dimensional NOESY experiments with short mixing times and chemical shift temperature dependencies it was possible to sequence-specifically assign all the β-CH_2 protons of the cysteines that bind the cluster and the α-CH protons of Cys8 and Cys14 in $FdII_{int}$. The sequence-specific assignment of the binding cysteines was also completed for $FdII_{ox}$ with the assignment of the α-CH proton of Cys50.

The change in behaviour of the temperature dependencies for $FdII_{int}$ compared with $FdII_{ox}$ indicated that the structure, specifically the Fe–Sγ–Cβ–Cα dihedral angles, near the [3Fe–4S] cluster changes. In order to model the temperature dependencies of the β-CH_2 protons for $FdII_{int}$ new *A* values need to be introduced.

Experiments to calculate the *A* values for both oxidized states need to be carried out (electron spin echo envelope modulation spectroscopy can be very useful in this matter, and will be pursued). The results obtained will allow a full understanding of the modifications in $FdII_{int}$ and calculation of the parameters that characterize the coupling between the irons in the cluster. A full structural characterization of the changes occurring in the $FdII_{int}$ state is under way.

It can be concluded that the electronic properties of the [3Fe–4S] cluster are essentially modulated by the 'constraints' imposed by the polypeptide chain of the protein.

It is remarkable that such a small protein, FdII, containing a 3Fe cluster and an internal disulfide bridge can be an electron sink ($3e^-$ at the cluster and $2e^-$ at the S–S bond). Such a multiple redox device can play unexpected roles in electron transfer and iron storage, considering also the easy cluster conversion processes (3Fe↔4Fe) that may take place under physiological conditions [41].

Acknowledgements We would like to thank Ludwig Krippahl for his help with the computer software provided by him and used in this work. This work was supported by Fundação para a Ciência e Tecnologia and COST D2 1.

References

1. Holm RH (1992) Advances in inorganic chemistry, vol 38. Academic, San Diego
2. Johnson MK (1994) Encyclopedia of inorganic chemistry. In: King RB (ed) Wiley, Chichester, pp 1896–1915
3. Beinert H, Holm RH, Munck E (1997) Science 277:653–659
4. Beinert H (2000) J Biol Inorg Chem 5:2–15
5. Glaser T, Hedman B, Hodgson KO, Solomon EI (2000) Acc Chem Res 33:859–868
6. Noodleman L, Case DA (2000) Adv Inorg Chem 33:423–470
7. Calzolai L, Zhou Z-H, Adams MWW, LaMar GN (1996) J Am Chem Soc 118:2513–2514
8. Hunsicker-Wang LM, Heine A, Chen Y, Luna EP, Todaro T et al (2003) Biochemistry 42:7303–7317
9. Flint DH, Allen RM (1996) Chem Rev 96:2315–2334
10. Beinert H, Kennedy MC, Stout CD (1996) Chem Rev 96:2335–2373
11. Jarret JT (2003) Curr Opin Chem Biol 7:174–182
12. Cheek J, Broderick JB (2001) J Biol Inorg Chem 6:209–226
13. Dobbek H, Svetlitchnyi V, Gremer L, Huber R, Meyer O (2001) Science 293:1281–1285
14. Crane BR, Siegel LM, Getzoff ED (1995) Science 270:59–67
15. Doukov TI, Iverson TM, Seravalli J, Ragsdale SW, Drennan CL (2002) Science 298:567–572
16. Darnault C, Volbeda A, Kim EJ, Legrand P, Vernede X et al (2003) Nat Struct Biol 10:271–279
17. Svetlichnyi V, Dobbek H, Meyer-Klaucke W, Meins T, Thiele B et al (2004) Proc Natl Acad Sci USA 101:446–451
18. Nicolet Y, Cavazza C, Fontecilla-Camps JC (2002) J Inorg Biochem 91:1–8
19. Peters JW, Lanzilotta WN, Lemon BJ, Seefeldt LC (1998) Science 282:1853–1858
20. Thauer RK, Schönheit P (1982) Iron-sulfur proteins. In: Spiro TG (ed) Wiley-Interscience, New York, pp 329–341
21. Plank DW, Kennedy MC, Beinert H, Howard JB (1989) J Biol Chem 264:20385–20393
22. Golinelli MP, Chatelet C, Duin EC, Johnson MK, Meyer J (1998) Biochemistry 37:10429–10437
23. Mulholland SE, Gibney BR, Rabanal F, Dutton PL (1998) J Am Chem Soc 120:10296–10302
24. Cunningham RP, Asahara H, Bank JF, Scholes CP, Salerno JC et al (1989) Biochemistry 28:4450–4455
25. Kuo CF, McRee DE, Fisher CL, O'Handley SF, Cunningham RP, Tainer JA (1992) Science 258:434–440
26. Porello SL, Cannon MJ, David SS (1998) Biochemistry 37:6465–6475
27. Guan Y, Manuel RC, Arvai AS, Parikh SS, Mol CD et al (1998) Nat Struct Biol 5:1058–1064
28. Kiley PJ, Beinert H (2003) Curr Opin Microbiol 6:181–185
29. Demple B, Ding H, Jorgensen M (2002) Methods Enzymol 348:355–364
30. Alen C, Sonenshein AL (1999) Proc Natl Acad Sci USA 96:10412–10417
31. Tang Y, Guest JR (1999) Microbiology 145:3069–3079
32. Smith JL, Zaluzec EJ, Wery JP, Niu L, Switzer RL et al (1994) Science 264:1427–1433
33. Wu CK, Dailey HA, Rose JP, Burden A, Sellers VM, Wang BC (2001) Nat Struct Biol 8:156–160
34. Sellers VM, Johnson MK, Dailey HA (1996) Biochemistry 35:2699–2704
35. Dai S, Schwendtmayer C, Schurmann P, Ramaswamy S, Eklund H (2000) Science 287:655–658
36. Duin EC, Madadi-Kahkesh S, Hedderich R, Clay MD, Johnson MK (2002) FEBS Lett 512:263–268
37. Walters EM, Johnson MK (2004) Photosynth Res 79:249–264
38. Ugulave NB, Gibney BR, Jarret JT (2001) Biochemistry 40:8343–8351
39. Berkovitch F, Nicolet Y, Wan JT, Jarret JT, Drennan CL (2004) Science 303:76–79
40. Jameson GN, Cosper MM, Hernandez HL, Johnson MK, Huynh BH (2004) Biochemistry 43:2022–2031
41. Moura JJG, Macedo A, Palma PN (1994) Ferredoxins. Methods in enzymology. In: Peck HD Jr, LeGall J (eds) Inorganic microbial sulphur metabolism, vol 243. Academic, New York, chap 12
42. Bruschi M, Hatchikian C, LeGall J, Moura JJG, Xavier AV (1976) Biochem Biophys Acta 449:275–284
43. Bruschi M (1979) Biochim Biophys Res Commun 91:623
44. Kissinger CR, Sieker LC, Adman ET, Jensen JH (1991) J Mol Biol 219:693–715
45. Goodfellow BJ, Macedo AL, Rodrigues P, Wray V, Moura I, Moura JJG (1999) J Biol Inorg Chem 4:421–430
46. Macedo AL, Moura I, Surerus KK, Papaefthymiou V, Liu M, LeGall J, Münck E, Moura JJG (1994) J Biol Chem 269:8052–8058
47. Moura JJG, Moura I, Kent TA, Lipscomb JD, Huynh BH, LeGall J, Xavier AV, Münck E (1982) J Biol Chem 257:6259–6267
48. Moura I, Moura JJG, Münck E, Papaefthymiou V, LeGall J (1986) J Am Chem Soc 108:349–351
49. Butt JN, Sucheta A, Breton J, Thomson AJ, Hatchikian EC (1991) J Am Chem Soc 113:8948–8950
50. Conover RC, Park J-B, Adams MWW, Johnson MK (1990) J Am Chem Soc 112:4562–4564
51. Surerus KK, Münck E, Moura I, Moura JJG, LeGall J (1987) J Am Chem Soc 109:3805–3807
52. Moreno C, Macedo AL, Moura I, LeGall J, Moura JJG (1994) J Inorg Biochem 53:219–234
53. Hsieh YC, Liu MY, LeGall J, Chen CJ (2005) Acta Crystallogr D 61:780–783
54. Kent TA, Huynh BH, Münck E (1980) Proc Natl Acad Sci USA 77:6574
55. Emptage MH, Kent TA, Huynh BH, Rawlings J, Orme-Johnson WH, Münk E (1980) J Biol Chem 255:1793–1796
56. Xavier AV, Moura JJG, Moura I (1981) Struct Bonding 43:187–213
57. Armstrong FA, Butt JN, George SJ, Hatchikian EC, Thomson AJ (1989) FEBS Lett 259:15
58. Shen B, Martin LL, Butt JN, Armstrong FA, Stout CD, Jensen GM, Stephens PJ, LaMar GN, Gorst CM, Burgess BK (1993) J Biol Chem 268:25929–25939
59. Breton JL, Duff JL, Butt JN, Armstrong FA, Petillot Y, Forest E, Schafer G, Thomson AJ (1995) Eur J Biochem 233:937–946
60. Smith ET, Blamey JM, Zhou ZH, Adams MWW (1995) Biochemistry 53:219–234
61. Macedo AL, Palma N, Moura I, LeGall J, Wray V, Moura JJG (1993) Magn Res Chem 31:S59–S67
62. Macedo AL, Moura I, LeGall J, Huynh B, Moura JJG (1993) Inorg Chem 32:1101–1105
63. Bertini I, Ciurli S, Luchinat C (1995) Struct Bonding 83:1–53
64. Noodleman L (1988) Inorg Chem 27:3677–3679
65. Aono S, Bertini I, Cowan JA, Luchinat C, Rosato A, Viezolli MS (1996) J Biol Inorg Chem 1:523–528
66. Bertini I, Dikiy A, Luchinat C, Macinai R, Viezolli MS, Vincenzini M (1997) Biochemistry 36:3570–3579

67. Gorst CM, Zhou ZH, Ma K, Teng Q, Howard JB, Adams MWW, LaMar GN (1995) Biochemistry 34:8788–8795
68. Vold RL, Waugh JS, Klein MP, Phelps DE (1968) J Chem Phys 48:3831
69. Inubushi T, Becker EDJ (1983) J Magn Res 51:128–133
70. Bertini I, Briganti F, Luchinat C, Scozzafava A, Sola M (1991) J Am Chem Soc 113:1237–1245
71. Macura SR, Ernst RR (1980) Mol Phys 40:95–117
72. Kumar A, Ernst RR, Wüthrich K (1980) Biochem Biophys Res Commun 95:1
73. Busse SC, LaMar GN, Yu LP, Howard JB, Smith ET, Zhou ZH, Adams MWW (1992) Biochemistry 31: 11952–11962
74. Donaire A, Gorst CM, Zhou ZH, Adams MWW, LaMar GN (1994) J Am Chem Soc 116:6841–6849
75. Cheng H, Grohmann K, Sweeney W (1992) J Biol Chem 267:8073–8080
76. Davy SL, Osborne MJ, Breton J, Moore GR, Thomson AJ, Bertini I, Luchinat C (1995) FEBS Lett 363:199–204
77. Imai T, Matsumoto T, Ohta S, Ohmori D, Suzuki K, Tanaka J, Tsukioka M, Tobari J (1983) Biochim Biophys Acta 743:91–97
78. Trower MK, Marshall JE, Doleman MS, Emptage MH, Sariaslani FS (1990) Biochim Biophys Acta 1037:290–296
79. Bertini I, Capozzi F, Luchinat C, Piccioli M, Vila AJ (1994) J Am Chem Soc 116:651–660
80. Werth MT, Kurtz Jr DM, Moura I, LeGall J (1987) J Am Chem Soc 109:273–275
81. Rodrigues P, Graça F, Macedo AL, Moura I, Moura JJG (2001) Biochem Biophys Res Commun 289:630–633